Available online at www.sciencedirect.com
SCIENCE DIRECT®
Journal of Sound and Vibration 289 (2006) 779–806
JOURNAL OF SOUND AND VIBRATION
www.elsevier.com/locate/jsvi

Dispersive elastodynamics of 1D banded materials and structures: analysis

Mahmoud I. Hussein, Gregory M. Hulbert*, Richard A. Scott

Department of Mechanical Engineering, The University of Michigan, Ann Arbor, MI 48109, USA

Received 6 August 2004; received in revised form 16 February 2005; accepted 20 February 2005
Available online 5 May 2005

Abstract

The elastodynamics of 1D periodic materials and finite structures comprising these materials are studied with particular emphasis on correlating their frequency-dependent characteristics and on elucidating their pass-band and stop-band behaviors. Dispersion relations are derived for periodic materials and are employed in a novel manner for computing both pass-band and stop-band complex mode shapes. Through simulations of harmonically induced wave motion within a finite number of unit cells, conformity of the frequency band structure between infinite and finite periodic systems is shown. In particular, only one or two unit cells of a periodic material could be sufficient for "frequency bandedness" to carry over from the infinite periodic case, and only three to four unit cells are necessary for the decay in normalized transmission within a stop band to practically saturate with an increase in the number of cells. Dominant speeds in the scattered wave field within the same finite set of unit cells are observed to match those of phase and group velocities of the infinite periodic material within the most active pass band. Dynamic response due to impulse excitation also is shown to capture the infinite periodic material dynamical characteristics. Finally, steady-state vibration analyses are conducted on a finite fully periodic structure revealing a conformity in the natural frequency spread to the frequency band layout of the infinite periodic material. The steady-state forced response is observed to exhibit mode localization patterns that resemble those of the infinite periodic medium, and it is shown that the maximum localized response under stop-band conditions could be significantly less than in an equivalent homogenous structure and the converse is true for pass-band conditions.

*Corresponding author. Tel.: +1 734 763 4956; fax: +1 734 747 3170.
E-mail address: hulbert@umich.edu (G.M. Hulbert).

0022-460X/$ - see front matter © 2005 Elsevier Ltd. All rights reserved.
doi:10.1016/j.jsv.2005.02.030

1. Introduction

An important class of composite materials is one in which the individual constituents are geometrically laid out in a periodic fashion, where each repeated unit is referred to as a *unit cell*. This importance stems from the fact that there are several practically promising dynamical characteristics that periodic composite materials (henceforth referred to as *periodic materials*) possess. This arises from their frequency-dependent wave propagation characteristics described by the frequency spectra, that is, mappings between temporal *frequency* and *wavenumber*.

Due to their dispersive nature, some periodic materials may exhibit distinct frequency ranges in which effective wave propagation is not permitted to take place. These frequency ranges are commonly referred to as *band gaps* or *stop bands*. The remaining frequency ranges are called *pass bands*, where, as the terminology implies, waves are allowed to "pass" or propagate through the medium. The location of these bands in the frequency domain, and the form of the dispersion relation within these bands, make up the *frequency band structure* of the periodic material.

A promising technological development revolves around employing periodic materials in forming engineering structures. The term *structure* here is distinguished from the term *material*. A structure has definite size and boundaries, and can be mechanically loaded (e.g., by application of force), whereas a material has indefinite size, typically modeled or expressed pointwise, and does not permit any form of loading. Recognizing that the dynamic behavior in both stop-band and pass-band frequencies is exploitable motivates the use, hereafter, of the phrases "banded materials/structures" as opposed to "band-gap materials/structures".

A brief chronological literature survey (not exhaustive) is now presented. The study of wave propagation in periodic media was effectively pioneered by Floquet in 1883 [1] when he studied a 1D Mathieu's equation involving temporal, rather than spatial, periodicity. Subsequently, Rayleigh [2] arrived at a form of Floquet's theorem through his derivation of a solution for waves in 1D periodic media. His findings revealed the notion of a band gap. Bloch [3] presented a theorem generalizing Floquet's results to spatial periodicity in three dimensions showing that the wave field in a periodic medium is also periodic up to a phase multiplier. A rigorous geometric interpretation of wave diffractions was provided by Brillouin [4]. In the 1950s, a substantial number of theoretical investigations in solid state physics focused on band structures of solids. By the late 1960s, band theory gained considerable credibility once theorists and experimentalists correlated their results (see Ref. [5] for band theory in solid state physics).

In the field of elasticity, several studies were conducted on wave propagation in stratified solid media in the early 1950s, e.g., Thomson's [6] use of matrices to study plane elastic waves in such media and Haskell's [7] employment of the same approach for surface waves. In 1973, Lee and Yang [8] used Floquet's theorem in their treatment of 1D wave propagation in elastic periodic composites. They generated periodic displacement profiles and interpreted properties of Floquet waves in terms of normal modes. The band-gap feature and properties at band ends were among the focal points of their work.

The existence of a band gap in a realistic 3D crystal was "suggested" in the seminal papers of Yablonovitch [9] and John [10]. Shortly after, Ho et al. [11] developed a plane-wave expansion method and used it to demonstrate a full photonic (electromagnetic) band gap for dielectric spheres arranged in the diamond structure. At that stage it was established that some crystalline microstructures are indeed capable of forbidding the transmission of waves, be they electronic,

photonic, or phononic (vibrational), at band-gap frequency ranges. A large number of papers have since appeared in this area (see, e.g., Refs. [12,13], and Ref. [14] for a review). Substantial research has also been conducted on a similar class of problems, that is, homogenous structures with periodic boundary conditions (see, e.g., Refs. [15–17]).

Returning to 1D periodically layered media, the case where more than two sub-layers, of two or more constituent materials, are present in a periodic material's unit cell was the focus of the work presented by Esquivel-Sirvent and Cocoletzi [18] and Shen and Cao [19]. They combined the transfer matrix method with Floquet's theorem to predict the dispersion curves across a specified frequency range. Martinsson and Movchan [20] studied band gaps in the context of infinite lattice structures with continuous elements. They correlated characteristics of oscillators within the unit cell with those of the periodic system as a whole.

The above studies focused primarily on infinite domains. Research has also been conducted on finite models of periodic systems, which is of practical importance. Schemes were proposed in which the transfer matrix method is used to predict the frequency-dependent vibration transmission across a 1D finite periodic structure embedded in a base material [21,22]. These schemes, however, are limited to a plane wave solution and do not permit the consideration of realistic loading and boundary conditions. Substantial coverage of wave propagation in 1D periodic structures, infinite and finite, is available in Ref. [23] in which the method of characteristics was used. No attention was given, however, to the effects that the number of unit cells in a finite structure has on the wave propagation characteristics, and there was no consideration of the spatial behavior.

The most elaborate studies to date in which the effects of the number of unit cells on the dynamics of a bounded structure were considered are those of Jensen [24] and Hussein et al. [25]. In the former, these effects on the steady-state forced response were considered in the context of fully periodic spring-mass systems. Also considered were the effects of boundaries, viscous damping and imperfections. In the latter, a brief analysis was provided on the effects of the numbers of cells forming a periodic waveguide wall on the overall guide performance. Some preliminary results on the effects of "finiteness" in 1D periodic structures for both transient and steady-state dynamics was presented in Refs. [26,27]. A comprehensive and frequently updated list of articles on topics involving sonic, as well as photonic, band gaps is compiled by Dowling, et al. [28].

The goal of this paper is to provide additional analysis and understanding of the pass-band/stop-band dispersive behavior of linear elastic periodic materials and structures with a perspective on not only the frequency domain but also the temporal and spatial domains, including speeds of wave propagation. Furthermore, this paper focuses on correlating the dynamic response of the respective infinite and finite systems. More specifically, the dynamical characteristics (frequency bands and mode shapes) of a periodic material are correlated with the dynamic response of a structure that is composed of a finite number of unit cells of the same periodic material. An aim of this correlation is the establishment of conditions on the number of periodic unit cells required for a qualitative similarity in behavior to take place. Steady-state vibration analyses of fully bounded (i.e., more realistic) periodic structures are also considered in order to provide a modal analysis perspective on banded structures. Here, total wave reflections take place at the periodic domain boundaries. Particular emphasis is placed on the behavior of the closest unit cell from the location of excitation because a seemingly high degree of possibly damaging mode localization takes place near the loading point.

Attention is focused on 1D models since they provide a platform for rigorous analysis of the fundamental dynamical processes that pertain to periodically heterogeneous materials and structures without indulging in the complexities associated with multiple directionality. Furthermore, from a practical perspective, 1D models may be realized as *layered* materials and structures, which are fairly economical to manufacture.

In the next section, the governing equations for linear elastodynamics are presented for a heterogeneous solid. In Section 3, a solution method for the infinite periodic material problem is described and an algorithm is given in the Appendix for predicting spatial profiles (mode shapes) across an arbitrary number of unit cells. Section 4 outlines solutions methods for the finite periodic structure problem. Numerical examples are provided in Section 5. Analyses are conducted on an arbitrarily chosen periodic layered material, and subsequently on structures composed of this composite material. The degree to which the size and location of frequency bands (i.e., frequency "bandedness") carry through from material to structure is investigated, and the effect of "finiteness" on wave attenuation is studied. Furthermore, observable velocities of wave propagation in a periodic structure are correlated with corresponding phase and group velocity values from the periodic material's dispersion curves. In addition to cases involving harmonic excitations, the dynamics resulting from the application of a general transient pulse load are also studied. Finally, free and steady-state forced vibration analyses of a finite periodic structure are carried out in order to compare the modal distribution, and mode localization patterns, with those associated with the infinite periodic material. Conclusions are drawn in Section 6.

2. Governing equation for linear elastodynamics

The governing equation of motion for longitudinal wave propagation in a 1D heterogeneous solid is

$$\rho\ddot{u} = \sigma_{,x} + f, \tag{1}$$

where $\rho = \rho(x)$, $f = f(x,t)$, $\sigma = \sigma(x,t)$, and $u = u(x,t)$ denote density, external force, stress, and displacement, respectively. The position coordinate and time are respectively denoted by x and t. A superscript $(\cdot)_{,x}$ denotes differentiation with respect to position, while a superposed dot denotes differentiation with respect to time. Assuming linear elastic material,

$$\sigma = Eu_{,x}, \tag{2}$$

where $E = E(x)$ is the elastic modulus. The following subsections include the statements for the various problems considered in this work. It should be noted that while only longitudinal wave propagation is considered, the given problem statements (and subsequent analysis procedures) are easily extendable to transverse wave motion.

2.1. Infinite periodic layered materials

A periodically layered composite material is described by the configuration of an infinitely repeated unit cell that consists of sublayers of different constituent material properties and thicknesses. Hence, analysis of a periodic material requires consideration of a solution domain that consists only of a single unit cell. A schematic of a unit cell is presented in Fig. 1 where an

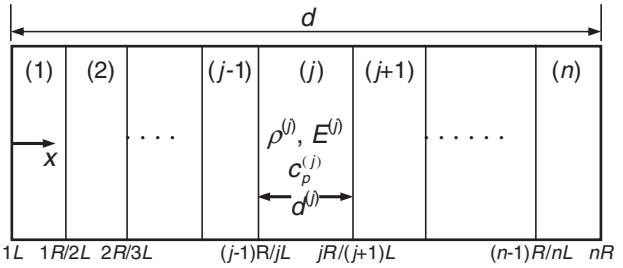

Fig. 1. Unit cell consisting of n layers. The layer number is indicated in parenthesis. A material property of a layer (j) is denoted $(.)^{(j)}$. The boundaries of each layer are identified by an index as shown. For example, the right boundary of layer 1 is identified as $1R$, or $2L$ since it is also the left boundary of layer 2.

arbitrary layer j is shown to be positioned between an adjacent layer $j-1$ at its left and an adjacent layer $j+1$ at its right. The unit cell has length d. The jth layer has thickness $d^{(j)}$, density $\rho^{(j)}$, elastic modulus $E^{(j)}$, and longitudinal velocity $c^{(j)}$, where $c^{(j)} = \sqrt{E^{(j)}/\rho^{(j)}}$. The boundary conditions that must be satisfied at the layer interfaces are (i) continuity of the displacement u and (ii) continuity of the stress σ. Furthermore, no external forces are permitted, i.e., $f = 0$ in Eq. (1).

The solution $u = u(x,t)$ in the jth layer is written as a superposition of forward and backward traveling waves with harmonic time dependence:

$$u(x,t) = [A_+^{(j)} e^{ik^{(j)}x} + A_-^{(j)} e^{-ik^{(j)}x}] \times e^{-i\omega t}, \tag{3}$$

where $i = \sqrt{-1}$, $k^{(j)} = \omega/c^{(j)}$ and ω is the temporal frequency. The stress component is given by Eq. (2). The objective is to compute the frequency spectrum and displacement profiles (mode shapes) that characterize the dispersive dynamics of a given unit cell (hence that of the periodic material as a whole).

2.2. Finite periodic or partially periodic layered structures

For finite structures, two types of problems are considered. The first focuses on a bounded partially periodic structure with a time-varying load applied at one end. This is an initial boundary value problem defined by Eq. (1) and an appropriate set of initial and boundary conditions. Two loading configurations in the form of prescribed displacements are considered: harmonic displacement, and a transient pulse (prescribed displacement loading implies that $f = 0$ in Eq. (1)). Direct time integration is performed to obtain the solution. The objective here is two-fold: (i) to investigate the effects of "finiteness" and the number of cells on the dynamic response, and (ii) to analyze the dispersive wave propagation (including wave velocities) in the periodic region of the structure. The periodic region is located at the end where the load is applied, and the remaining part (which is sufficiently long) consists of a homogenous material to absorb waves exiting from the periodic region. This layout facilitates carrying out both the above studies without allowing wave reflects from external boundaries to interfere in the analysis.

The second type of problem considered is that of classical vibration analysis of a finite fully periodic structure subjected to harmonic forcing. The governing equation again follows exactly

the form given in Eq. (1), but now it is assumed that the applied force is harmonic at frequency ω^*, that is,

$$f(x,t) = F(x,\omega^*)\mathrm{e}^{\mathrm{i}\omega^* t}, \tag{4}$$

and the forced vibration response is

$$u(x,t) = U(x,\omega^*)\mathrm{e}^{\mathrm{i}\omega^* t}, \tag{5}$$

where F and U are generally a complex coefficient carrying frequency-dependent magnitude and phase information. Substituting Eqs. (4)–(5) into Eqs. (1)–(2) gives

$$-\omega^2\rho U = (EU_{,x})_{,x} + F. \tag{6}$$

With an appropriate set of boundary conditions, Eq. (6) forms a boundary value problem. The natural frequencies and modes shapes of the same bounded finite structure can be obtained by setting $f = 0$, and solving the following eigen problem:

$$-\omega^2\rho U = (EU_{,x})_{,x} + \text{Boundary Conditions}. \tag{7}$$

In addition to incorporating the effects of the external boundaries, this problem setup provides information on the steady-state dynamics of the structure. At steady state, the dispersion phenomenon across the periodic unit cells is no longer evolving, and hence a more representative picture of the overall behavior of the structure is given.

3. Solution methods

In this section, solution methods are described for both the problem of an infinite periodic material and the problem of a finite periodic, or partially periodic, structure.

3.1. Material problem

3.1.1. Transfer matrix method for a multi-layered unit cell

The transfer matrix method [18] is used to model the mechanical behavior of a 1D multi-layered unit cell. Eqs. (1)–(2) can be written in matrix form as ($\mathrm{e}^{-\mathrm{i}\omega t}$ omitted)

$$\begin{bmatrix} u(x) \\ \sigma(x) \end{bmatrix} = \begin{bmatrix} 1 & 1 \\ \mathrm{i}Z^{(j)} & -\mathrm{i}Z^{(j)} \end{bmatrix} \begin{bmatrix} A_+^{(j)}\mathrm{e}^{\mathrm{i}k^{(j)}x} \\ A_-^{(j)}\mathrm{e}^{-\mathrm{i}k^{(j)}x} \end{bmatrix} = \mathbf{B}_j \begin{bmatrix} A_+^{(j)}\mathrm{e}^{\mathrm{i}k^{(j)}x} \\ A_-^{(j)}\mathrm{e}^{-\mathrm{i}k^{(j)}x} \end{bmatrix}, \tag{8}$$

where $Z^{(j)} = \rho^{(j)}c^{(j)^2}k^{(j)}$. Let x^{jL} and x^{jR} denote the position along the x-axis of the left and right boundaries of layer j, respectively. Using Eq. (8) and the relation $x^{jR} = x^{jL} + d^{(j)}$, the values of the displacement u and traction (stress) σ at x^{jL} are related to those at x^{jR}:

$$\begin{bmatrix} u(x^{jR}) \\ \sigma(x^{jR}) \end{bmatrix} = \mathbf{B}_j \begin{bmatrix} \mathrm{e}^{\mathrm{i}k^{(j)}d^{(j)}} & 0 \\ 0 & \mathrm{e}^{-\mathrm{i}k^{(j)}d^{(j)}} \end{bmatrix} \begin{bmatrix} A_+^{(j)}\mathrm{e}^{\mathrm{i}k^{(j)}x^{jL}} \\ A_-^{(j)}\mathrm{e}^{-\mathrm{i}k^{(j)}x^{jL}} \end{bmatrix}. \tag{9}$$

Setting $\mathbf{D}_j(d^{(j)}) = \mathrm{diag}[\exp(\mathrm{i}k^{(j)}d^{(j)}), \exp(-\mathrm{i}k^{(j)}d^{(j)})]$, and using Eq. (8), Eq. (9) is rewritten as

$$\begin{bmatrix} u(x^{jR}) \\ \sigma(x^{jR}) \end{bmatrix} = \mathbf{B}_j\mathbf{D}_j(d^{(j)})\mathbf{B}_j^{-1}\begin{bmatrix} u(x^{jL}) \\ \sigma(x^{jL}) \end{bmatrix} = \mathbf{T}_j\begin{bmatrix} u(x^{jL}) \\ \sigma(x^{jL}) \end{bmatrix}, \tag{10}$$

where $\mathbf{T}_j$ is a 2×2 *transfer matrix* for layer j, and is defined as

$$\mathbf{T}_j = \mathbf{B}_j\mathbf{D}_j(d^{(j)})\mathbf{B}_j^{-1}. \tag{11}$$

Upon expanding Eq. (11), $\mathbf{T}_j$ has the following form:

$$\mathbf{T}_j = \begin{bmatrix} \cos(k^{(j)}d^{(j)}) & (1/Z^{(j)})\sin(k^{(j)}d^{(j)}) \\ -Z^{(j)}\sin(k^{(j)}d^{(j)}) & \cos(k^{(j)}d^{(j)}) \end{bmatrix}. \tag{12}$$

Since the construction of the transfer matrix $\mathbf{T}_j$ is valid for any layer, the result presented in Eq. (10) can be extended recursively to relate the displacements and the stresses across several layers. Consider a complete unit cell consisting of n layers as shown in Fig. 1. Defining

$$\mathbf{y}(x) = \begin{bmatrix} u(x) \\ \sigma(x) \end{bmatrix}, \tag{13}$$

then the transfer matrix mapping across all n layers can be written compactly as

$$\begin{aligned} \mathbf{y}(x_1^{1R}) &= \mathbf{T}_1\mathbf{y}(x_1^{1L}), \\ &\vdots \\ \mathbf{y}(x_1^{nR}) &= \mathbf{T}_n\mathbf{T}_{n-1}\cdots\mathbf{T}_1\mathbf{y}(x_1^{1L}). \end{aligned} \tag{14}$$

The last line in Eq. (14) shows that the displacement and traction at the left boundary of the first layer in a unit cell are related to those at the right boundary of the nth layer by

$$\begin{bmatrix} u \\ \sigma \end{bmatrix}_{x^{nR}} = \mathbf{T}\begin{bmatrix} u \\ \sigma \end{bmatrix}_{x^{1L}}, \tag{15}$$

where

$$\mathbf{T} = \mathbf{T}_n\mathbf{T}_{n-1}\cdots\mathbf{T}_1. \tag{16}$$

$\mathbf{T}$ will be referred to as the *cumulative transfer matrix*.

3.1.2. Calculation of dispersion curves

Consider a multi-layered material composed of a repetition of a single n-layered unit cell. The length, d, of the unit cell defines the material's periodicity:

$$d = d^{(1)} + d^{(2)} + \cdots + d^{(n)}. \tag{17}$$

Floquet's theorem relates the time harmonic response at a given point in a unit cell to the corresponding point in an adjacent unit cell. This relation is given by

$$\mathbf{y}(x + d) = \mathrm{e}^{\mathrm{i}kd}\mathbf{y}(x), \tag{18}$$

where k is a wavenumber that corresponds to the global "effective" wave field across the periodic medium. Setting $x = x^{jL}$ allows equating Eqs. (15) and (18) which leads to the following eigen problem:

$$[\mathbf{T} - \mathbf{I}e^{ikd}]\mathbf{y}(x^{1L}) = \mathbf{0}. \tag{19}$$

Eq. (19) can be rewritten as

$$\mathbf{T}(\omega)\mathbf{y}(x^{1L}) = \lambda\mathbf{y}(x^{1L}), \tag{20}$$

where $\lambda = \exp(ikd)$ is a complex eigenvalue and $\mathbf{y}(x^{1L})$ is a complex eigenvector. The solution of Eq. (20), which appears in complex conjugate pairs, provides dispersion curves (plots of ω versus k) for longitudinal wave propagation in the infinite periodic material characterized by the cumulative transfer matrix $\mathbf{T}$.

3.1.3. Characteristics of the dispersion relation

Wavenumbers computed from Eq. (20) are real and positive in certain frequency ranges and strictly imaginary at other ranges. In general, the wavenumber can be written as

$$k = k_{\text{real}} - ik_{\text{imaginary}}, \tag{21}$$

where k_{real} and $k_{\text{imaginary}}$ are real numbers. The sign in Eq. (20) could alternatively be selected as positive, i.e., $k = k_{\text{real}} + ik_{\text{imaginary}}$. The choice of definition of k and the choice of the eigenvalue in Eq. (20) (among the two complex conjugate pairs) together should result in an attenuating solution within stop bands. The displacement and stress components of $\mathbf{y}$ in Eq. (20) are also complex to account for both magnitude and spatial phase. Following the definition of Eq. (21), consider the two classes of frequency ranges outlined above:

Class 1: $k = k_{\text{real}}$, $k_{\text{real}} > 0$.

From Eq. (18),

$$\mathbf{y}(x+d) = e^{ikd}\mathbf{y}(x),$$

$$\mathbf{y}(x+d) = e^{i|k_{\text{real}}|d}\mathbf{y}(x). \tag{22}$$

Eq. (22) indicates that the displacement and stress at positions x and $x+d$ (i.e., corresponding locations in adjacent unit cells) differ only by a phase factor $e^{i|k_{\text{real}}|d}$. This indicates that waves are effectively "allowed" to travel at the ranges of frequencies belonging to this class, forming frequency pass bands.

Class 2: $k = -ik_{\text{imaginary}}$, $k_{\text{imaginary}} < 0$.

From Eq. (18),

$$\mathbf{y}(x+d) = e^{ikd}\mathbf{y}(x),$$

$$\mathbf{y}(x+d) = e^{-|k_{\text{imaginary}}|d}\mathbf{y}(x). \tag{23}$$

Eq. (23) indicates that the displacement and stress at positions x_1 and $x_1 + d$ do not have a phase difference, and furthermore, there is a spatial exponential attenuation in magnitude of strength proportional to $|k_{\text{imaginary}}|$. Thus, waves in these frequency ranges are effectively "forbidden" from traveling, forming frequency stop bands.

3.1.4. Mode shapes

In this section, the displacement and stress mode shapes associated with both pass-band and stop-band wave motion in the 1D infinite periodic layered material are considered. The eigenvalues and eigenvectors of Eq. (20) determine these time-dependent mode shapes.

For a given pair of complex amplitudes $A_+^{(j)}$ and $A_-^{(j)}$, the displacement and stress within each unit cell layer can be computed using Eq. (8). Within adjacent unit cells, these quantities can be computed using Floquet's theorem, Eq. (18), which is restated for a series of unit cells as

$$\mathbf{y}(x+rd)_{l+r} = \mathrm{e}^{\mathrm{i}krd}\mathbf{y}(x)_l, \quad l, r \text{ integer}, \tag{24}$$

where the subscripts $(\cdot)_l$ and $(\cdot)_{l+r}$ refer to the lth and $(l+r)$th unit cell, respectively. An algorithm is presented in the Appendix for computing the mode shapes.

3.2. Structure problem

Using a standard finite element method, Eq. (1) leads to the following algebraic equation:

$$\mathbf{M}\ddot{\mathbf{D}} + \mathbf{K}\mathbf{D} = \mathbf{F}, \tag{25}$$

where the **M** and **K** matrices are the stiffness and mass matrices, respectively, and **D** and **F** are the nodal displacement and force vectors, respectively. In this study, Eq. (25) is time integrated using a standard explicit central difference scheme. In the integration process, an exact solution is obtained if the discrete time step (denoted Δt) is chosen such that the Courant–Friedricks–Levy (CFL) number lies at the stability limit, i.e., $\Delta t = \Delta h^e/c^{(j)}$ (where Δh^e is the element size). If the time step is chosen such that $\Delta t < \Delta h^e/c^{(j)}$, some accuracy is compromised but stability is still guaranteed.

The boundary value problem whose governing equation is Eq. (6) is also discretized using the finite element method leading to the following algebraic equation:

$$(-\omega^2\mathbf{M} + \mathbf{K})\mathbf{D} = \mathbf{F}. \tag{26}$$

The solution of Eq. (26) is the particular solution, or the frequency-dependent steady-state forced vibration response. Similarly, Eq. (7) is discretized to give

$$\mathbf{K}\mathbf{D} = \lambda\mathbf{M}\mathbf{D}, \tag{27}$$

where **D** is now the eigenvector.

4. Analysis: Examples of layered materials and structures

In this section, the dynamics of periodic layered materials and structures with an arbitrarily chosen unit cell configuration is considered as an example case. The unit cell is composed of two layers of stiff (fiber) and compliant (matrix) materials, as shown in the left inset in Fig. 2. Using 'f' and 'm' to denote fiber and matrix, respectively, the dimensions are $d_f/d = 0.8$, and the material property ratios are $\rho_f/\rho_m = 3$ and $E_f/E_m = 12$. Note that the dispersive characteristics of a periodic composite is determined by the ratios of material properties, and not the absolute properties of the individual constituents.

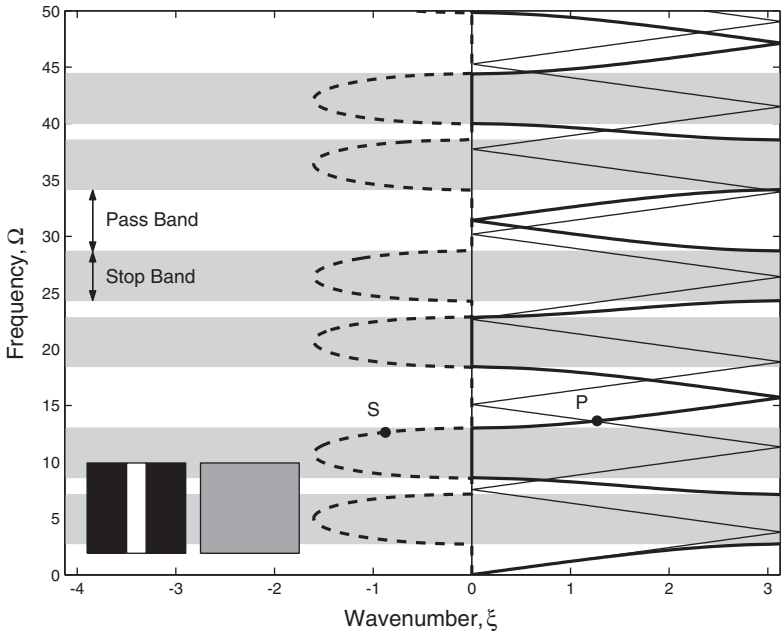

Fig. 2. Frequency spectrum for periodic and equivalent homogenous unit cells. Stop bands are shaded, and points P and S are chosen for further analysis. Unit cell layouts are presented in insets, where black represents stiff (fiber) material, white represents compliant (matrix) material, and gray represents equivalent homogenous material. (——) Periodic (real part), (– –) periodic (imaginary part), (——) homogenous.

4.1. Material problem

4.1.1. Frequency spectra and mode shapes

Using the transfer matrix method and Floquet's theorem, the frequency spectrum in the considered infinite periodic material is shown in Fig. 2. The plot spans a frequency range of $0 \leqslant \Omega \leqslant 50$, where $\Omega = \omega d/\sqrt{E_m/\rho_m}$ is a non-dimensional frequency. This frequency range was discretized into 1001 sample points. The abscissa is given by the non-dimensional wave number $\xi = k \times d$. The value $\xi = \pi$ represents the limit of what is known as the first Brillouin zone (see Ref. [4]). Beyond this value, non-dimensional frequency repeats every π multiples of ξ. The existence of multiple branches in the frequency spectrum is noticeable. Physically, each "higher" branch represents frequency values at higher wavenumbers. For example, the second branch spans $\pi \leqslant \xi \leqslant 2\pi$.

The nonlinearity of the curves indicates that the medium is dispersive. Frequencies corresponding to real-valued wavenumbers are associated with pass-band modes, and frequencies matching complex or pure imaginary wavenumbers are associated with stop-band modes. The formation of such a banded frequency spectrum is a manifestation of mechanisms of wave interference that take place due to wave scatter and dispersion. Within the interior (as well as the surface) space of the periodic material, waves scatter (i.e., transmit and reflect) across constituent material interfaces, and subsequently disperse into more waves which in turn effectively interfere

in a constructive (i.e., adding up) or destructive (i.e., canceling) manner. The former process occurs at the pass-band frequencies, and the latter at the stop-band frequencies. For purposes of comparison, a homogeneous medium having statically equivalent averaged elastic modulus, E_{avg} and density, ρ_{avg} of the heterogeneous unit cell is considered (see right inset in Fig. 2), and its spectrum is computed and superimposed in Fig. 2. The averaging is carried out using the rule of mixtures (see Eq. (28) for E_{avg} and Eq. (29) for ρ_{avg}).

$$E_{\text{avg}} = \left(\frac{d_f}{d}\frac{1}{E_f} + \frac{d_m}{d}\frac{1}{E_m}\right)^{-1}, \tag{28}$$

$$\rho_{\text{avg}} = \frac{1}{d}(d_f\rho_f + d_m f_m). \tag{29}$$

It is clear that the homogeneous material is non-dispersive, and is therefore not frequency-banded.

Two points, P and S, are marked in Fig. 2. Point P lies at a pass-band frequency ($\Omega = 13.6$) while Point S lies at a stop-band frequency ($\Omega = 12.6$). Using the scheme presented in the Appendix, the mode shapes corresponding to these points were computed over a range of five unit cells and over a period. Note that as given in Eq. (A.1) in the Appendix, the displacement at the reference spatial location ($x = 0$) is given as a time harmonic function. Fig. 3 shows two "snap shots" of the response separated by a time phase of $T/8$, where $T = 2\pi/\omega$. It is observed that the pass-band effective wave is traveling (note the phase difference) and non-attenuating across the unit cells (Fig. 3a), whereas that of the stop band is standing and attenuating (Fig. 3b). The results shown agree with Floquet's theorem. Recall that the full modes may not span the length of an integer number of unit cells since the periodicity of the response is e^{ikd} and not d. The corresponding modes shapes for an equivalent homogenous medium are superimposed in the respective graphs. Note the differences in spatial profile, as well as phase, compared to the dispersed fields.

4.2. Structure problem

From a practical point of view, it is important to examine the relevance of the computed dispersion curves and mode shapes of a periodic material to the dynamic properties of a structure composed of a finite number of periodic unit cells. To explore the dynamic effects pertaining to finite periodicity, a bounded structure is considered that consists of a finite number, N_{Cell}, of the heterogeneous unit cell shown in Fig. 2. In Sections 4.2.1 and 4.2.2, wave propagation analyses are presented for cases involving (i) harmonic excitation, and (ii) impulse excitation, respectively. In Section 4.2.3, free and steady-state forced vibration analyses are performed.

4.2.1. Wave motion analysis: harmonic excitation

For wave motion analysis, the finite structure is chosen to consist of N_{Cell} periodic unit cells, but also to have a substantially large portion composed of a homogenous material (e.g., the same stiff material of the periodic portion) and located adjacent to the right (receiving) end of the periodic region as depicted in Fig. 4a. A prescribed harmonic displacement at a specified frequency is applied at the left end, $u(0,t) = e^{i\omega t}$, $t \geqslant 0$, and a time simulation of the wave motion is generated by solving the initial boundary value (whose discretized equation of motion is Eq. (25)) using the

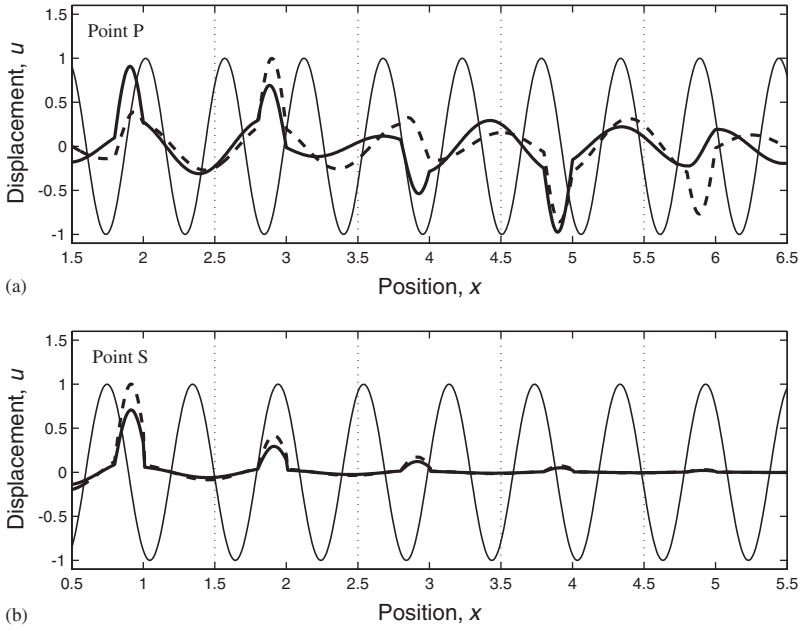

Fig. 3. Two time "snap shots" of portions of modes shapes spanning five unit cells corresponding to points (a) P, and (b) S. To facilitate comparison between the two cases, the viewing window is shifted such that the displacements at the left end of the plot for time t are approximately equal. Corresponding mode shapes for an equivalent homogenous medium are superimposed. Vertical, dotted lines mark boundaries of unit cells. (——) Periodic at time t, (– –) periodic at time $t + T/8$, (——) homogenous at time t.

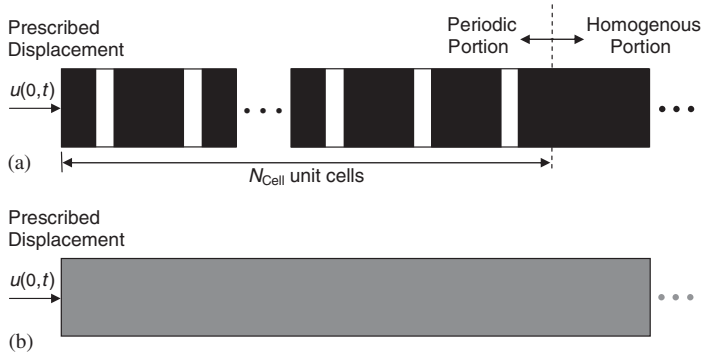

Fig. 4. (a) A structure partially consisting of a finite number, N_{Cell}, of periodic unit cells (black and white colors represent fiber and matrix, respectively). The homogenous portion is extended in length so that no waves are allowed to reflect back into the periodic portion throughout the duration of the simulation. Loading in the form of prescribed harmonic displacement is applied at the left end. (b) Equivalent homogenous structure.

numerical integration technique referred to in Section 3.2. The size of the homogenous portion of the structure is chosen to be large enough so that waves are not reflected back to the periodic region from the right end of the homogenous portion during the prescribed simulation time. In

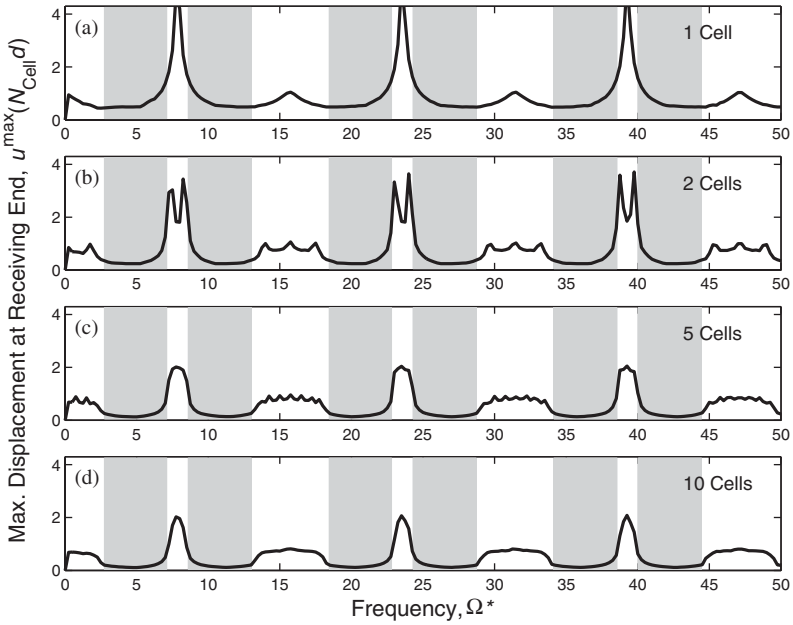

Fig. 5. Transmissibility, defined as $u_1^{\max}(N_{\text{Cell}}d)$, of finite periodic portion of structure shown in Fig. 4a as a function of excitation frequency. The number of unit cells, N_{Cell}, composing the periodic portion is (a) 1, (b) 2, (c) 5 and (d) 10. Stop bands for corresponding infinite periodic medium are shaded.

this manner, external boundary effects at the right end are removed from the analysis. The periodic portion of the model is divided into 150 piecewise linear finite elements, with lengths satisfying the condition $\Delta h_f^e = 2\Delta h_m^e$. This number of finite elements achieves convergence for all the analyses presented in Sections 4.2.1 and 4.2.2. A time step of $\Delta t = \Delta h^e/c = 0.01$ s is used. The analysis is repeated over the frequency range $0 \leqslant \Omega^* \leqslant 50$, the same range covered in Section 4.1.

4.2.1.1. Effects of "finiteness". Conducting analyses for different values of N_{Cell} provides information on the effects of "finiteness" on (i) the frequency band layout, that is, how well the frequency bands match those of the infinite periodic material, and (ii) the degree of wave attenuation that takes place within stop bands. The maximum displacement at the end of the N_{Cell}th unit cell over a total simulation duration of T_{Tot} seconds (i.e., $|u^{\max}(N_{\text{Cell}}d)|$, where $u^{\max} = \max_t(u)$) is chosen to represent the transmissibility of the periodic region. In Fig. 5, this quantity is plotted versus excitation frequency for the range $0 \leqslant \Omega \leqslant 50$, $T_{\text{Tot}} = 10$, and for $N_{\text{Cell}} = 1, 2, 5, 10$. The value of $T_{\text{Tot}} = 10$ is sufficient for considerable scattering and dispersion to take place so that the effects of the frequency bands are apparent (but not sufficiently long for wave reflects from the right end to occur). The stop-band frequency ranges for the infinite periodic material are shaded in Fig. 5 to facilitate comparison. First, it observed that the response of finite periodic structures is frequency-banded and generally conforms with the band layout of the infinite periodic material (i.e., high at pass bands and low at stop bands). This result means that finite periodicity in itself does not destroy the frequency-banded nature of the dynamic response. It also implies that the wave interference mechanisms that take place within periodic unit cells

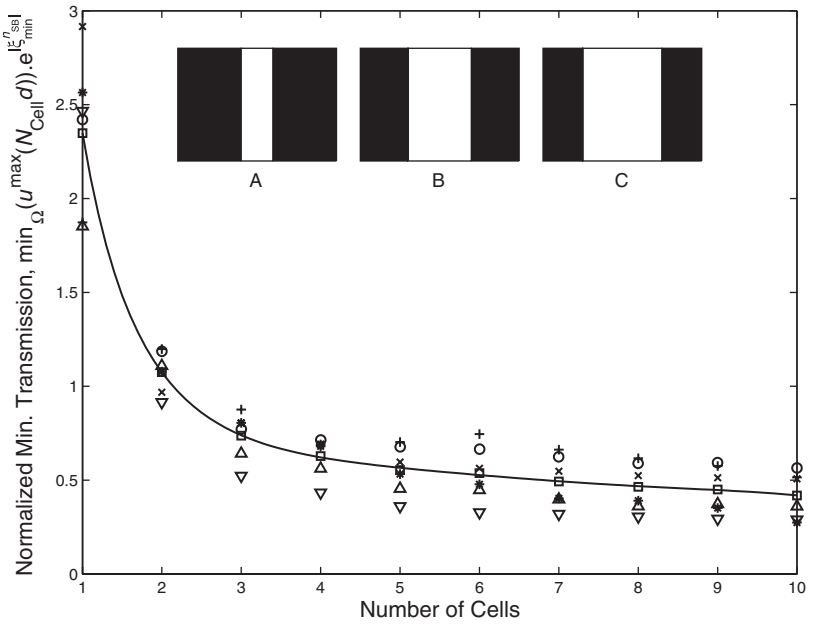

Fig. 6. Normalized minimum transmission across excitation frequency range spanning first stop band versus number of unit cells, N_{Cell}, composing the finite periodic portion of structure shown in Fig. 4a. Results for six unit cell designs as well as a curve fit of the average are shown. The unit cell geometric layouts are shown in the insets. (◯) A, $\rho_f/\rho_m = 3$, (×) A, $\rho_f/\rho_m = 15$, (+) B, $\rho_f/\rho_m = 3$, (•) B, $\rho_f/\rho_m = 15$, (△) C, $\rho_f/\rho_m = 3$, (▽) C, $\rho_f/\rho_m = 15$, (□) Average, (——) Fit.

(and that are responsible for creating stop bands and pass bands) are achieved within a confined periodic region. Second, it is apparent that more cells lead to sharper frequency bands and higher conformity with the band layout of the infinite periodic material. However, note that with only one unit cell of the periodic material (for the case considered), the transmission peaks within the pass-band frequency ranges, especially the narrow ones. With only two unit cells, the transmission follows closely the frequency band layout of the periodic material (i.e., there is a clear jump in amplitude within pass bands).

It is of practical interest to arrive at some general trend for the relationship between transmission and number of unit cells within a finite structure. In the following analysis, a total of six different unit cell designs are considered. The three cell geometric layouts (labeled A, B and C) shown in the inset of Fig. 6 are used with two different density ratios ($\rho_f/\rho_m = 3$ and $\rho_f/\rho_m = 15$) considered for each, hence a total of six designs. The ratio of elastic moduli is kept constant for all designs, e.g., $E_f/E_m = 12$. Let n_{SB} denote the stop-band number. The same time simulations are conducted on each of these designs as in Fig. 5. In post-processing the data, the minimum value of transmission over the frequency range of the lowest ($n_{\text{SB}} = 1$) stop band, i.e., $\min_\Omega(u^{\max}(N_{\text{Cell}}d))$, is normalized by multiplying with the exponent of the minimum value of the wavenumber at that same stop band ($\exp(\xi^{n_{\text{SB}}}_{\min})$, where $n_{\text{SB}} = 1$). In Fig. 6 this total quantity is plotted versus the number of unit cells for $N_{\text{Cell}} = 1, 2, \ldots, 10$ and for the six unit cell designs. The average of these six plots is calculated and the exponent of that average is curve fitted (in a least-squares sense)

using a 5th degree polynomial, that is,

$$\min_{\Omega}(u^{\max}(N_{\text{Cell}}d))\exp(\xi_{\min}^{n_{\text{SB}}}) = \exp(p_1N_{\text{Cell}}^5 + p_2N_{\text{Cell}}^4 + p_3N_{\text{Cell}}^3 + p_4N_{\text{Cell}}^2 + p_5N_{\text{Cell}} + p_6), \quad (30)$$

where $p_1, p_2, \ldots, p_6$ are coefficients. For the above analysis, $p_1 = -0.0000816$, $p_2 = 0.0027863$, $p_3 = -0.0375660$, $p_4 = 0.2516875$, $p_5 = -0.87107493$, $p_6 = 1.0251557$. It should be noted that these numbers will vary with different designs, number of designs considered, and value of n_{SB}. However, the overall trend shown by the fitted curve in Fig. 6 is expected to approximately hold for a large number of different designs, especially for $n_{\text{SB}} = 1$. It is observed that for all the reduction in normalized minimum transmission that 10 unit cells can cause, nearly 83% or 90% of it can be achieved when only 3 or 4 unit cells are available, respectively.

These results show that with knowledge of the minimum attenuation constant corresponding to a stop-band excitation frequency, $\xi_{\min}^{n_{\text{SB}}}$, the strength of attenuation in the finite structure could be approximately predicted as a function of the number of cells employed using

$$\min_{\Omega}(u^{\max}(N_{\text{Cell}}d)) = \exp(p_1N_{\text{Cell}}^5 + p_2N_{\text{Cell}}^4 + p_3N_{\text{Cell}}^3 + p_4N_{\text{Cell}}^2 + p_5N_{\text{Cell}} + p_6 - \xi_{\min}^{n_{\text{SB}}}). \quad (31)$$

4.2.1.2. Temporal, frequency and spatial response. A partially periodic structure of the configuration shown in Fig. 4a is chosen with $N_{\text{Cell}} = 5$. It is excited at a pass-band frequency of $\Omega^* = 13.6$ (Point P in Fig. 2), and at a stop-band frequency of $\Omega^* = 12.6$ (Point S in Fig. 2). The loading point is again at the left end and $T_{\text{Tot}} = 10$. With this 10 s total simulation duration, the observed fastest speed of wave propagation in the periodic portion corresponds to a total distance traveled that is approximately 43, and 40, times the wavelength for $\Omega^* = 13.6$, and $\Omega^* = 12.6$, respectively. These values suggest that considerable scattering and dispersion take place.

To examine the transmission characteristics across the 5 unit cells, both the time and frequency responses are computed at the left end (the input point) and at the end of the fifth unit cell (the output point). The frequency content is obtained by performing a fast Fourier transform (FFT) on the time signal spanning the 10 s duration. This is implemented using MATLAB [29]. Fig. 7 shows the input and output signals, in both the time and frequency domains, corresponding to excitation frequency $\Omega^* = 13.6$, and Fig. 8 shows the same information for $\Omega^* = 12.6$. It is observed that the output signal's maximum value is 72% of the input signal's amplitude for the pass-band case, and 18% for the stop-band case. Curves for the statically equivalent homogenous structure are superimposed.

The basic physical phenomena that are responsible for the creation of a banded frequency response can be also interpreted in terms of resonances. When the excitation frequency falls within a pass band, the input force (for the studied case of prescribed input displacement) is larger than that of stop-band cases due to impedance matching. The larger input force leads to larger structural response. Hence, the dynamics in the pass-band case exhibit the conditions of structural resonance. Note that the resonance conditions referred to here are local in the sense that they pertain to the periodic region only and not to the structure as whole.

Figs. 7 and 8 also show that the output response, for both the pass-band and stop-band cases, conforms to the frequency band structure of the corresponding infinite periodic medium. It is noteworthy that due to dispersion, the input energy spreads in the frequency spectrum and ends up at the receiving end with a content concentrated in all the pass bands within the frequency range considered. However, most of the transmission takes place through the closest pass bands

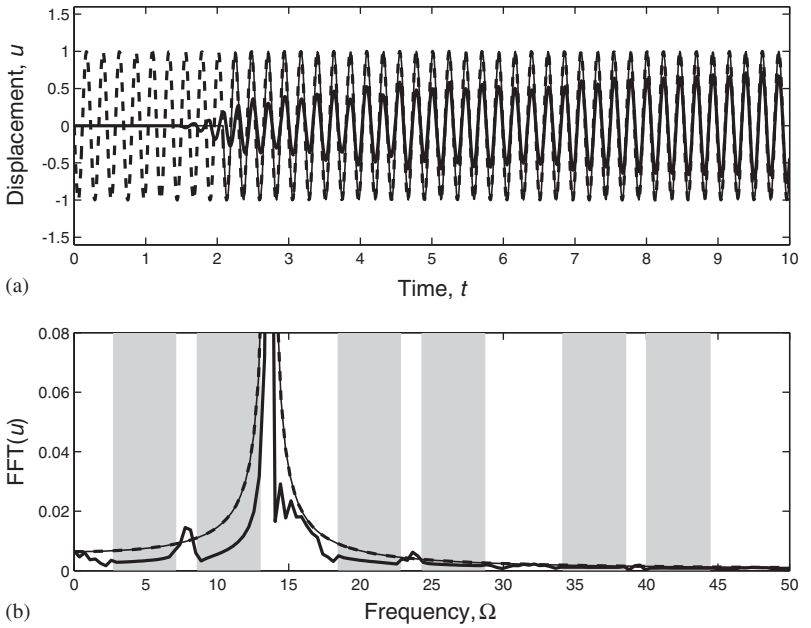

Fig. 7. "Input" and "Output" response in the (a) time and (b) frequency domains for structure shown in Fig. 4a. The excitation frequency is $\Omega^* = 13.6$ (within third pass band). The response of the equivalent homogenous structure is also shown. Stop bands for the corresponding infinite periodic medium are shaded. (– –) Input at left end, (——) output at end of fifth cell (periodic), (——) output at end of fifth cell (homogenous).

(whose modes get excited most). The same computational simulations are conducted on the equivalent homogenous structure, shown in Fig. 4b, and the results are superimposed in Figs. 7 and 8. Obviously, no frequency filtering takes place within homogenous structures.

The spatial response at the end of the simulation ($t = 10$ s) for the same pass-band and stop-band cases is shown in Figs. 9a and b, respectively. It is noticeable that the spatial profiles for both cases resemble the corresponding mode shapes within the infinite medium (see Fig. 3). This observation is importance because it demonstrates that the Floquet result approximately holds for a finite number of cells. This in turn suggests that the spatial profile in a bounded periodic structure (consisting possibly of a very large number of cells) can be predicted by analysis of only a single unit cell. The corresponding responses of the equivalent homogenous structure are superimposed in the same figures. It is clear that in the pass-band case, displacements are significantly larger—a characteristic of a resonant response—and no localizations occur across the periodic region. In the stop-band case, the peak displacement is within the first unit cell (closest to the loading point) and the profile rapidly attenuates across the remaining cells.

4.2.1.3. Wave speeds. Another feature of the dynamic response that can be studied via solution of the initial boundary-value elastodynamics problem are the dominant speeds of wave propagation. The finite partially periodic structure of Fig. 4a again is considered, but with $N_{\text{Cell}} = 10$. The structure is subjected to a time harmonic excitation load at the left end at a frequency of $\Omega^* = 5.5$, noting that this value is close to the center of the periodic material's first

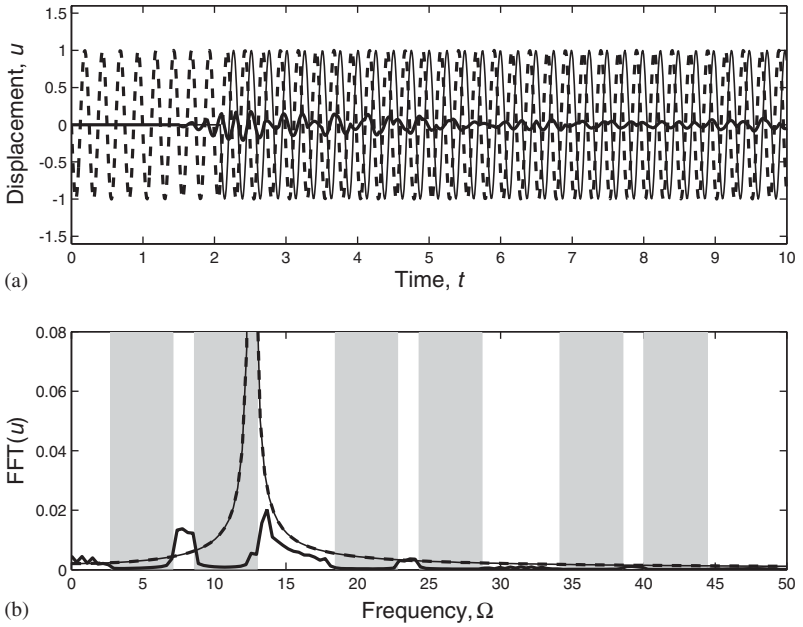

Fig. 8. "Input" and "Output" response in the (a) time and (b) frequency domains for structure shown in Fig. 4a. The excitation frequency is $\Omega^* = 12.6$ (within second stop band). The response of the equivalent homogenous structure is also shown. Stop bands for the corresponding infinite periodic medium are shaded. (– –) Input at left end, (——) output at end of fifth cell (periodic), (——) output at end of fifth cell (homogenous).

stop band. The "input" (at $x = 0$) and "output" (at $x = 10$) time and frequency signals are computed, and shown in Fig. 10. It is observed that most of the energy exits the ten-cell long periodic portion at a frequency range spanning the periodic material's second pass band. The time-evolving displacement field in the entire periodic region is plotted in Fig. 11. From this contour plot, two distinct wave fronts are observed: a fast traveling wave, and a slower higher amplitude wave. Note that theoretically there is a multitude of individual phase and group waves propagating in the structure because of dispersion. It is determined that the fast wave has a velocity of $\alpha_1 = 3.2$ unit lengths per second, and the slower wave has a velocity of $\alpha_2 = 1.3$ unit lengths per second.

The dispersion curves of the unit cell are shown in Fig. 12 in several forms. In Figs. 12c and d, the non-dimensional phase velocity, $\beta = c_p/\sqrt{E_m/\rho_m}$, $c_p = \omega/k$, and the non-dimensional group velocity,

$$\beta_g = \frac{\mathrm{d}\Omega}{d\xi}, \tag{32}$$

are respectively computed and plotted as a function of frequency. Upon studying these curves, it is realized that at the dominant propagation frequency range (i.e., around the center of the second pass band as shown in Fig. 10), the values of the phase ($c = 3.3$) and group ($c_g = 1.4$) velocities are almost identical to the corresponding observed values for wave propagation in the periodic region of the finite structure (i.e., $\alpha_1 = 3.2$ and $\alpha_2 = 1.3$, respectively). Hence, among the two most

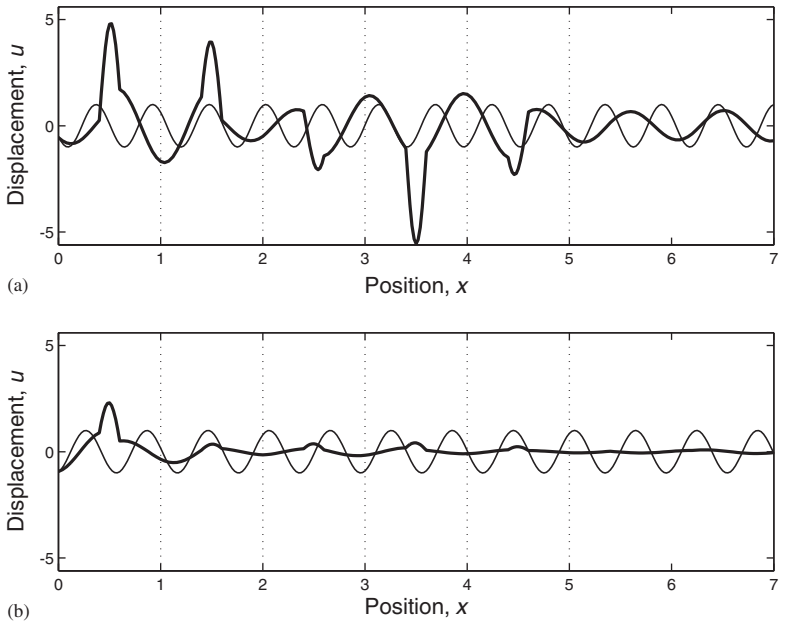

Fig. 9. Spatial distribution of wave field in structure shown in Fig. 4a at $t = 10$ s for excitation at (a) $\Omega^* = 13.6$ (within third pass band), and (b) $\Omega^* = 12.6$ (within second stop band). Non-dispersive wave fields in equivalent homogenous structure are superimposed. Vertical, dotted lines represent boundaries of unit cells. (——) Periodic, (——) homogenous.

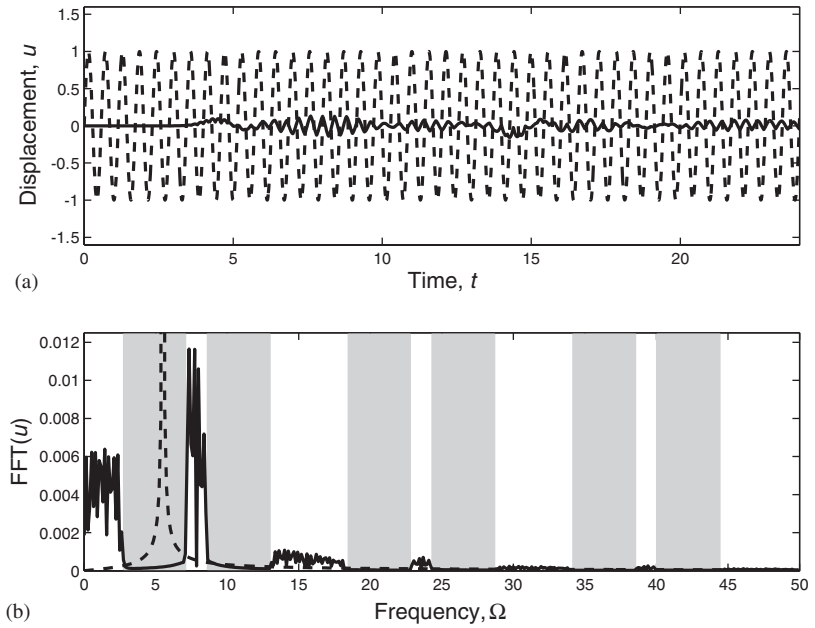

Fig. 10. "Input" and "Output" response in the (a) time and (b) frequency domains for structure shown in Fig. 4a. The excitation frequency is $\Omega^* = 5.5$ (within first stop band). Stop bands for the corresponding infinite periodic medium are shaded. (– –) Input at left end, (——) output at end of tenth cell.

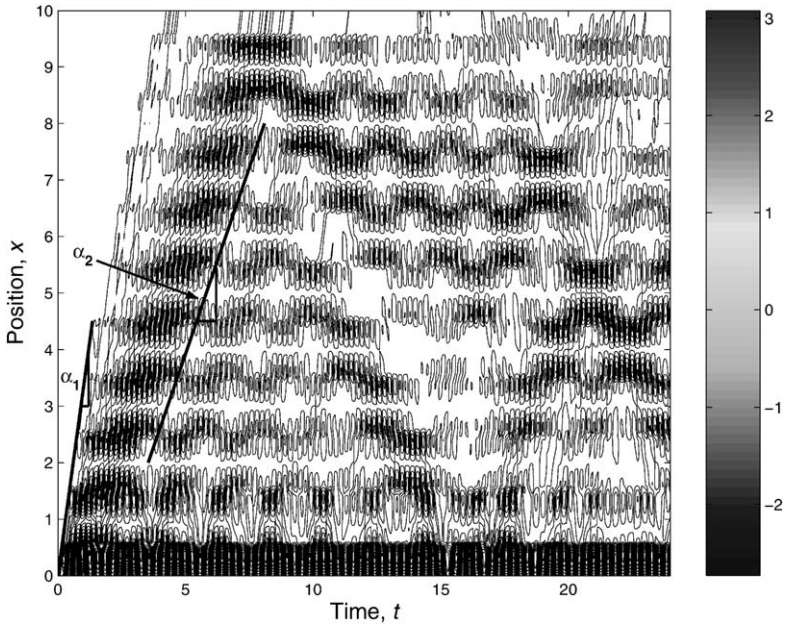

Fig. 11. Time–space displacement contour plot of wave field within structure shown in Fig. 4a. The vertical bar on the right provides a color index for values of displacement. The excitation frequency is $\Omega^* = 5.5$ (within first stop band). Two observable wave propagation "characteristic lines" are marked and the corresponding measured velocities are $\alpha_1 = 3.2$ and $\alpha_2 = 1.3$, respectively.

observable waves in the finite banded structure, the fastest one could be considered a phase wave, and the most intense one (which corresponds to energy propagation) could be considered a group wave. This result implies that the mapping of dynamical properties/characteristics from the infinite to the finite periodic structures also extends to speeds of wave propagation including the rate of energy propagation.

4.2.2. *Wave motion analysis: impulse excitation*

In this section, the finite partially periodic structure of Fig. 4a is subjected to a general impulse excitation. The spatial and temporal discretizations and the simulation duration are as in Section 4.2.1. The excitation is again applied as a prescribed displacement at the left end, and is chosen to have a double-Gaussian form, that is

$$f_{\mathrm{DG}}(t) = \mathrm{e}^{-a(t-b)^2} - \mathrm{e}^{-a(t-c)^2}, \tag{33}$$

where a, b and c are parameters. In order to synthesize a f_{DG} signal with a frequency content that approximately spans the range of interest $0 \leqslant \Omega^* \leqslant 50$, the parameters are chosen as follows:

$$a = 450,\ b = 0.25,\ c = 0.26. \tag{34}$$

Recall that this frequency range of interest spans the first six stop bands of the infinite periodic material. The results of the simulation are shown in the form of time and frequency responses in Fig. 13a and b, respectively, and in the form of a spatial response at $t = 10$ and a time envelope of

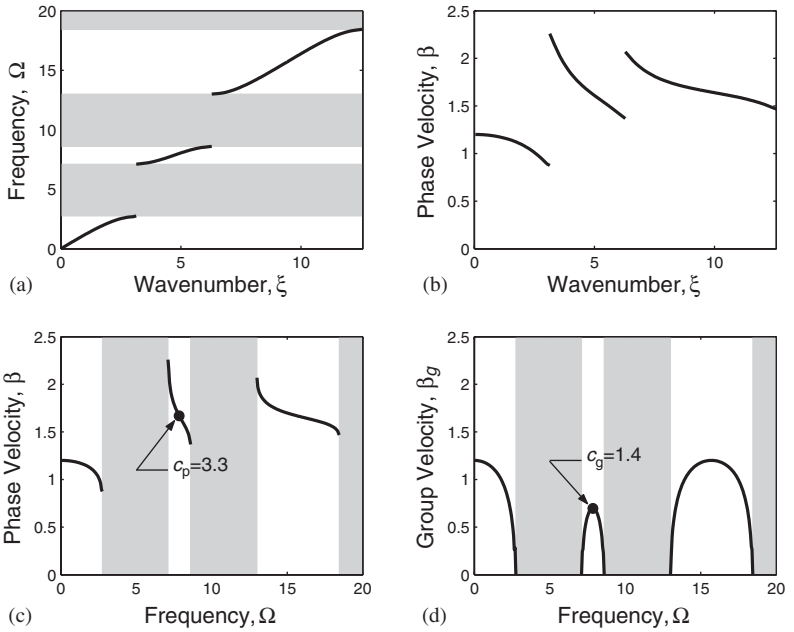

Fig. 12. Dispersion curves for unit cell composing periodic portion of structure shown in Fig. 4a: (a) frequency spectrum versus wavenumber, (b) phase velocity versus wavenumber, (c) phase velocity versus frequency, and (d) group velocity versus frequency. Stop bands are shaded in relevant graphs. The values (in dimensions of unit cells per second) of the phase and group velocities at the center of the second pass band are marked.

that response (i.e., maximum spatial response attained during the 10 s simulation duration) in Figs. 14a and b, respectively.

Fig. 13a shows that the "output" signal at the end of the fifth unit cell has been significantly suppressed (a maximum displacement that is 23% of the input displacement amplitude during the 10 s simulation time). Furthermore, the frequency content of the response (shown in Fig. 13b) at the same "output" position conforms very well to the band structure of the periodic material. In the equivalent homogenous structure, the shock load travels undisturbed as expected.

Fig. 14a indicates that after 10 s total simulation time, energy is still trapped within the periodic portion of the finite structure (i.e., motion is observed). For the equivalent homogenous structure, no motion is observed at that time instant because the waves have already passed the periodic portion as well as the homogenous region depicted in the figure. Fig. 14b suggests that a moderate level of localization of the maxima takes place within the first unit cell closest to the loading point.

4.2.3. Steady-state vibration analysis

In the previous section, waves are allowed to escape from the finite periodic region into the homogenous portion. In this section, a fully periodic structure is considered (see Fig. 15a). The structure is chosen to be composed of five unit cells of the same periodic material used in the previous sections. It is restrained from motion at the right end and is free to vibrate at the left end. Unlike the structure of Fig. 4a, the existence of a fixed boundary condition at the receiving end (i.e., the end of the fifth unit cell) causes all the transmitted waves to reflect back into the five

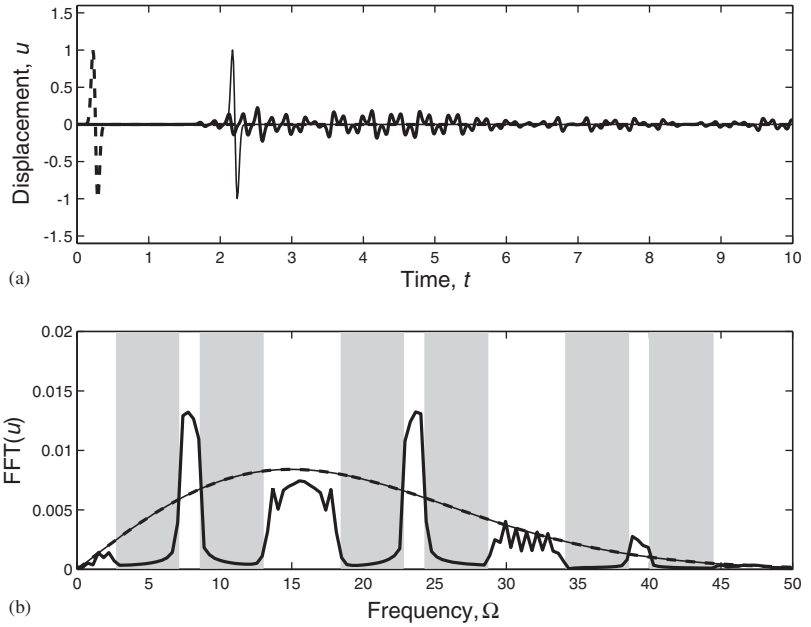

Fig. 13. "Input" and "Output" response in the (a) time and (b) frequency domains for structure shown in Fig. 4a. The loading is a prescribed displacement shock load (in double-Gaussian form) spanning $0 \leqslant \Omega^* \leqslant 50$ and is applied at the left end. Stop bands for the corresponding infinite periodic medium are shaded. (– –) Input at left end, (——) output at end of fifth cell (periodic), (——) output at end of fifth cell (homogenous).

periodic cells—which essentially constitute the entire structure. The finite element model of the structure consists of 600 piecewise linear elements, with lengths again following the condition $\Delta h_f^e = 2\Delta h_m^e$. A finer mesh is chosen in this section in order to accurately capture the high-frequency modes within the range $0 \leqslant \Omega \leqslant 50$.

4.2.3.1. Modal distribution. The natural frequencies of the structure are computed by solving the eigenproblem given in Eq. (27) and are plotted in Fig. 16. It is observed that these natural frequencies appear in clusters only in the pass bands in conformity with the frequency band layout of the corresponding infinite periodic medium (as depicted by the overlaying shaded stop band frequency ranges). For comparison purposes, the natural frequencies, Ω_n, of an equivalent homogenous structure (shown in Fig. 15b) with the same total mass and effective static stiffness are computed and also plotted in Fig. 16. Clearly, the non-dispersive homogenous structure is not frequency-banded. It can be observed that an increase in modal density for the periodic structure arises within the pass-band frequency ranges (to off-set the lack of modes within the adjacent stop bands). For example, within the fourth pass band, which spans the frequency range $22.8 \leqslant \Omega \leqslant 24.3$, the banded periodic structure has 5 modes compared to 2 for the equivalent homogenous structure. Another observation pertains to the overall dynamic stiffness of the two structures. With increase in frequency, the periodic structure's natural frequencies, on average, are increasingly larger than those of the equivalent homogenous structure. This indicates that the periodic structure is "dynamically" stiffer than its statically homogenized counterpart.

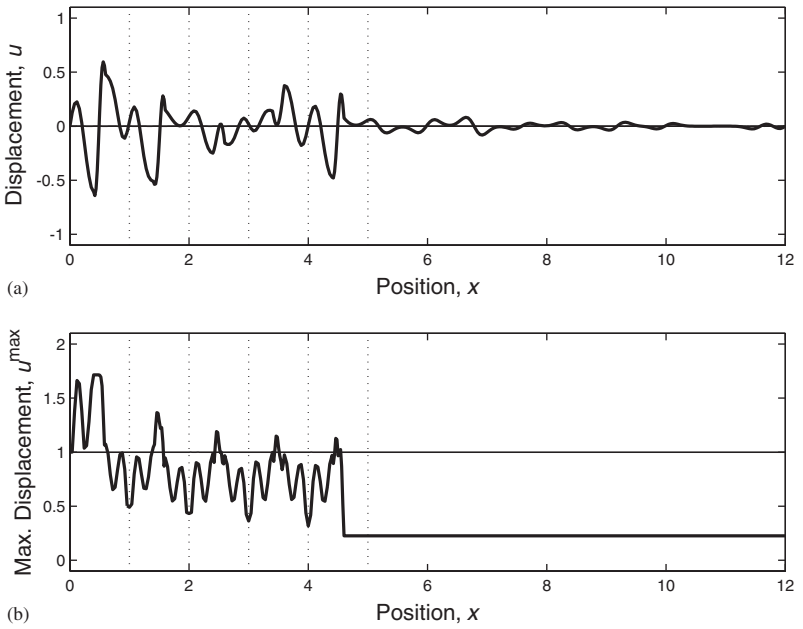

Fig. 14. (a) Spatial distribution of wave field in structure shown in Fig. 4a at $t = 10$ s when prescribed displacement double-Gaussian function spanning $0 \leqslant \Omega^* \leqslant 50$ is applied at the left end. (b) Envelope of maximum displacement within the structure throughout duration of simulation (10 s). Corresponding non-dispersive response of equivalent homogenous structure is superimposed. Vertical, dotted lines represent boundaries of unit cells. (——) Periodic, (——) homogenous.

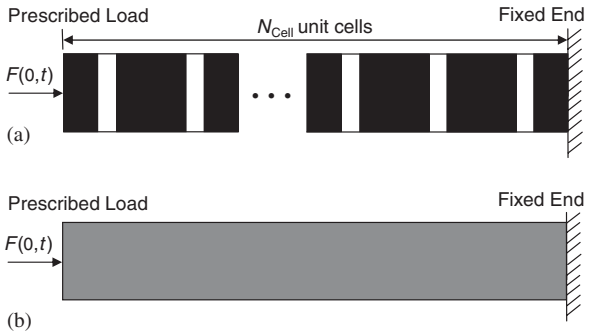

Fig. 15. (a) Finite periodic structure consisting of N_{Cell} unit cells (black and white colors represent fiber and matrix, respectively). The structure has a fixed boundary condition at the right end. At the left end, a prescribed harmonic force is applied. (b) Equivalent homogenous structure.

The same banded and homogenous structures of Fig. 15 are subjected to a load in the form of a prescribed harmonic forcing at the left end. The loading function is allowed to vary in frequency to cover the entire range, $0 \leqslant \Omega^* \leqslant 50$, considered in the previous analyses. The steady-state forced response is computed from the boundary-value problem whose discretized governing equation is

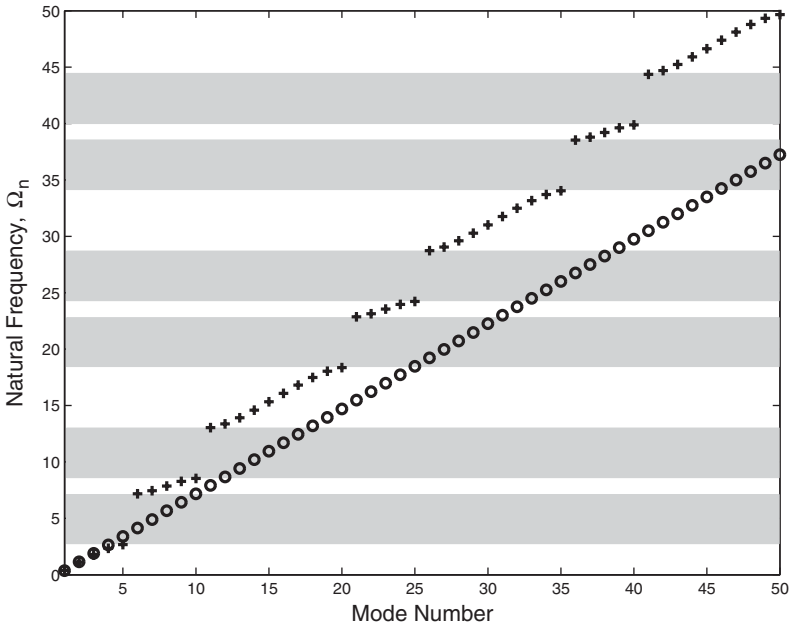

Fig. 16. Natural frequency spread for finite periodic structure and for equivalent homogenous structure. Stop bands for periodic material are shaded. (+) Periodic, (◯) homogenous.

Eq. (26). As a measure of the overall vibratory response, the root-mean-square value of all finite element nodal displacements is plotted in Fig. 17, and the maximum displacement values within the first and fifth unit cells are plotted in Fig. 18. The frequency sampling rate in these figures is $\Delta\Omega = 0.1$, and all displacement values are normalized with respect to $\delta = 5Fd/E_{\text{avg}}$, the static deflection of the equivalent homogenous structure. The infinite periodic material's stop-band frequency ranges are shaded in both these figures. Once again, the dynamic behavior of the finite periodic structure conforms to the infinite periodic material's frequency bands—and since as many as five unit cells are available, the attenuation at stop-band frequencies is significant (see Section 4.2.1.1). The reduced response within the stop bands indicates a form of anti-resonance taking place at these frequencies. When compared to the response of the equivalent homogenous structure (which is superimposed in Figs. 17 and 18), the banded structure is seen to vibrate at significantly lower values within most of the frequency range of each stop band. Note that in Fig. 18 it is shown that this is the case not only for vibrations at the receiving end but also within the first unit cell where localization is highest. These results indicate that introduction of material periodicity enhances the anti-resonance properties through a reduction in response throughout the entire structure at stop-band frequencies, therefore providing a means of non-conventional, non-dissipative frequency-dependent vibration suppression.

It should be noted that a particular harmonic loading force can lead to an excitation of surrounding, possibly out-of-band, modes (because of non-zero values of modal force corresponding to these surrounding modes). Since modes are numerous within pass bands and non-existing within stop bands, as shown in Fig. 16, an excitation within a pass band is likely to

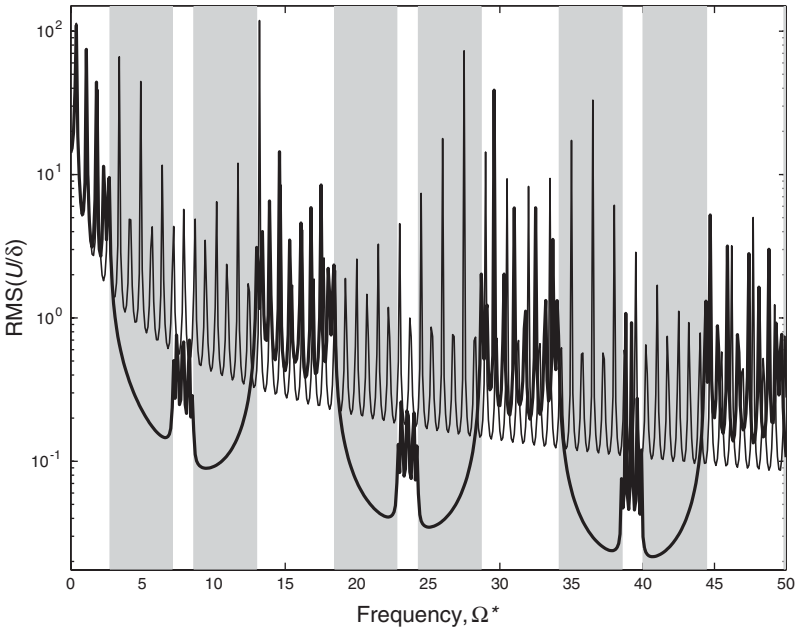

Fig. 17. Forced frequency response (root-mean-square of all finite element nodal displacements) for periodic structure and for equivalent homogenous structure. Stop bands for periodic material are shaded. (——) Periodic, (——) homogenous.

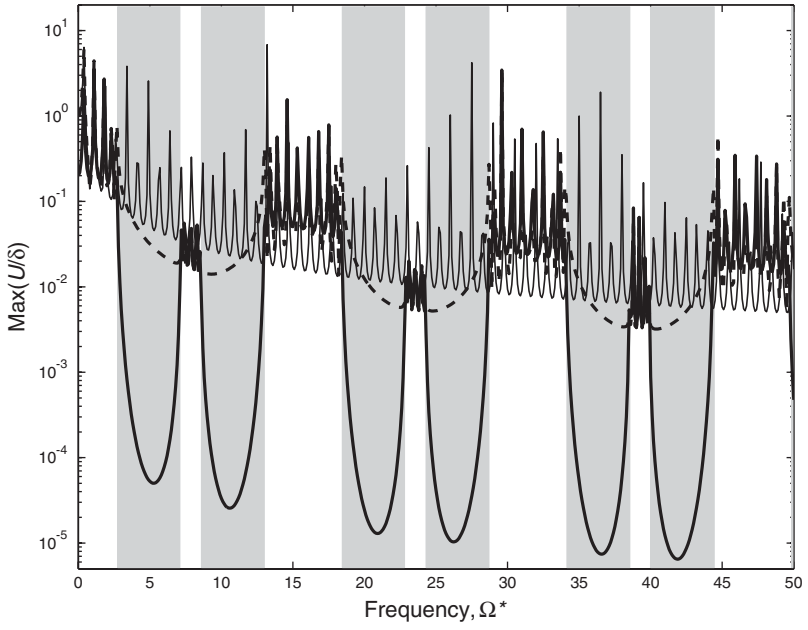

Fig. 18. Maximum displacement amplitude within first (leftmost) and fifth (rightmost) unit cells versus frequency of excitation. Corresponding results for equivalent homogenous structure are shown. Stop bands for periodic material are shaded. (– –) Within first cell, (——) within fifth cell, (——) homogenous.

significantly excite more modes than an excitation within a stop band. This is a "modal analysis" explanation for the reason the response shown in Figs. 17 and 18 is high within pass bands and low within stop bands. It also explains why the response can be relatively large at the boundaries of stop bands (due to neighboring pass-band frequencies). Furthermore, wide pass bands generally exhibit a larger response, compared to narrow pass bands, because the number of modes is greater in the wide pass bands. Since the modal distribution of the equivalent homogenous structure is relatively uniform, the corresponding forced response tends to be lower than the periodic structure's response within pass bands, and higher within stop bands.

4.2.3.2. Mode localization. To examine the spatial behavior of the considered finite periodic structure when excited at the pass-band and stop-band frequencies, the maximum displacements are plotted as a function of position. These results are presented in Fig. 19. It is seen that in the case of the pass-band frequency excitation, the response of the banded structure is high at more than one location and is non-decaying along the length of the structure. In contrast, the stop-band response is severely attenuated in space. The responses for the equivalent homogenous structure are superimposed to facilitate comparison of the spatial profile. Fig. 18 is to be referred to for comparison of frequency-dependent response amplitudes.

Finally, it is observed that like the responses shown in Fig. 9, the spatial displacement profiles in Fig. 19 have patterns that also resemble those of the infinite periodic medium which are presented in Fig. 3.

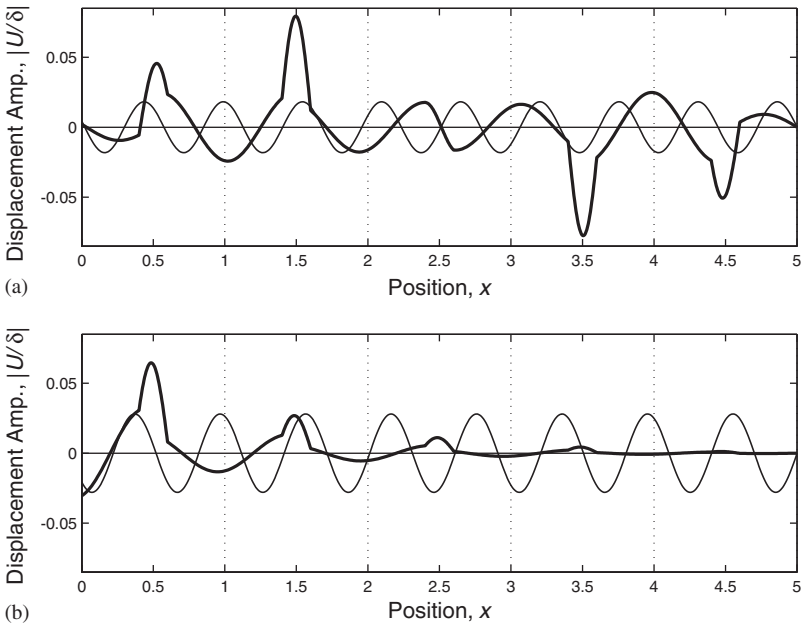

Fig. 19. Vibration response as a function of position in finite periodic structure for excitation at (a) $\Omega^* = 13.6$ (within third pass band), and (b) $\Omega^* = 12.6$ (within second stop band). Vertical, dotted lines represent boundaries of unit cells. (——) Periodic, (—) homogenous.

5. Conclusions

This paper focused on the analysis of the elastodynamics of infinite periodic materials and finite periodic structures. Using the transfer matrix method and Floquet's theorem, dispersion curves of a periodic medium with a multi-layered unit cell were computed, and a novel scheme was presented for obtaining both pass-band and stop-band mode shapes. A structure partially composed of a finite number of unit cells was then analyzed. A measure of wave transmission was computed as a function of frequency and for different numbers of unit cells. Conformity of the frequency band layout between infinite and finite periodic systems was analyzed. It is concluded that only one or two unit cells of a periodic material could be sufficient for "frequency bandedness" to carry over to a finite structure, and that no more than three or four unit cells are necessary for the decay in normalized transmission within a stop band to practically saturate with an increase in the number of cells. This congruence of response was demonstrated in the temporal, frequency and spatial domains for two transient (harmonic and impulse) loading cases as well as for steady-state vibrations. The analyses elucidated the pass-band and stop-band behaviors in finite structures. Match-up of velocities of wave propagation in the infinite and finite periodic domains was demonstrated as well. Furthermore, it was shown that even in regions of extreme mode localization, displacements of a periodic structure within stop bands can be significantly less than in an equivalent homogenous structure (and the converse is true for pass bands). These wave attenuation phenomena for periodic materials and structures can be exploited in structural design, which is the focus of a future paper.

Appendix

The following is an algorithm for calculating the displacement and stress mode shapes associated with both pass-band and stop-band wave motion in the 1D infinite periodic layered material.

Step 1: For a given ω, solve Eq. (20) for the eigenvalues $\lambda = \exp(\mathrm{i}kd)$ and the eigenvectors $\mathbf{y}(x^{1L})$. The eigensolution will appear in complex conjugate pairs. Select the appropriate solution considering the definition stated in Eq. (21).

Step 2: The eigenvector corresponds to the displacement and stress at the left boundary of an arbitrary unit cell l. To have a fixed frame of reference, the position x of this boundary will be set to zero, i.e., $x = 0$. Using Eq. (8), the eigenvector is expressed in the following form:

$$\mathbf{y}(x^{1L}) = \mathbf{B}_1 \begin{bmatrix} A_+^{(1)} \mathrm{e}^{\mathrm{i}k^{(1)}x^{1L}} \\ A_-^{(1)} \mathrm{e}^{-\mathrm{i}k^{(1)}x^{1L}} \end{bmatrix}. \tag{A.1}$$

Defining $\mathbf{a}_j = [A_+^{(j)} \; A_-^{(j)}]^{\mathrm{T}}$, and $\mathbf{C}_j(x^{jL}) = \mathrm{diag}[\mathrm{e}^{\mathrm{i}k^{(j)}x^{jL}}, \mathrm{e}^{-\mathrm{i}k^{(j)}x^{jL}}]$, Eq. (A.1) alternatively is written as

$$\mathbf{y}(x^{1L}) = \mathbf{B}_1 \mathbf{C}_1(x^{1L}) \mathbf{a}_1. \tag{A.2}$$

With the chosen reference frame, $x^{1L} = 0$, and $\mathbf{C}_1(x^{1L}) = \mathrm{diag}[1, 1] = I$, hence

$$\mathbf{y}(x^{1L}) = \mathbf{B}_1 \mathbf{a}_1. \tag{A.3}$$

Solve for $\mathbf{a}_1$ using Eq. (A.3)

$$\mathbf{a}_1 = \mathbf{B}_1^{-1}\mathbf{y}(x^{1L}).$$

Step 3: For $x = x^{2L}$,

$$\mathbf{y}(x^{2L}) = \mathbf{B}_2\mathbf{C}_2(x^{2L})\mathbf{a}_2, \tag{A.4}$$

and from Eq. (14),

$$\mathbf{y}(x^{2L}) = \mathbf{T}_1\mathbf{y}(x^{1L}). \tag{A.5}$$

Equate Eqs. (A.4) and (A.5)

$$\mathbf{T}_1\mathbf{y}(x^{1L}) = \mathbf{B}_2\mathbf{C}_2(x^{2L})\mathbf{a}_2. \tag{A.6}$$

Solve for the vector $\mathbf{a}_2$ using Eq. (A.2)

$$\mathbf{a}_2 = \mathbf{C}_2(x^{2L})^{-1}\mathbf{B}_2^{-1}\mathbf{T}_1\mathbf{B}_1\mathbf{a}_1. \tag{A.7}$$

Solve for the remaining vectors $\mathbf{a}_j$ (i.e., $\mathbf{a}_3, \ldots, \mathbf{a}_n$) in a similar manner

$$\mathbf{a}_j = \mathbf{C}_j(x^{jL})^{-1}\mathbf{B}_j^{-1}\mathbf{T}_j \ldots \mathbf{T}_2\mathbf{T}_1\mathbf{B}_1\mathbf{a}_1. \tag{A.8}$$

Step 4: The portion of the displacement and stress mode shapes within each layer in the first unit cell is computed from

$$\mathbf{y}(x) = \mathbf{B}_j\mathbf{C}_j(x)\mathbf{a}_j. \tag{A.9}$$

Step 5: Use Eq. (24) to compute the displacement and stress mode shapes over as many subsequent unit cells as desired. A full mode shape is realized when the displacement/stress profile spans a wavelength, $2\pi/k$, noting that the periodicity of the wave mode shape is related to the periodicity of the medium through the phase multiplier e^{ikd}. The magnitudes of the displacement and stress could be normalized using their respectively maximum values within a wavelength.

References

[1] G. Floquet, Sur les equations différentielles linéaries à coefficients périodiques, *annales de l'Ecole Normale Supérieur* 12 (1883) 47–88.

[2] L. Rayleigh, On the maintenance of vibrations by forces of double frequency, and on the propagation of waves through a medium endowed with a periodic structure, *Philosophical Magazine* 24 (1887) 145–159.

[3] F. Bloch, Über die Quantenmechanik der Electron in Kristallgittern, *Zeifschrift für Physik* 52 (1928) 555–600.

[4] L. Brillouin, *Wave Propagation in Periodic Structures*, second ed., Dover Publication, New York, 1953.

[5] C. Kittel, *Introduction to Solid State Physics*, Wiley, New York, 1996.

[6] W.T. Thomson, Transmission of elastic waves through a stratified solid medium, *Journal of Applied Physics* 21 (1950) 89–93.

[7] N.A. Haskell, The dispersion of surface waves on multilayered media, *Bulletin of the Seismological Society of America* (1952) 17–34.

[8] E.H. Lee, Wei H. Yang, H. Wei H, On waves in composite materials with periodic structure, *SIAM Journal of Applied Mathematics* 25 (3) (1973) 492–499.

[9] E. Yablonovitch, Inhibited spontaneous emission in solid-state physics and electronics, *Physical Review Letters* 58 (1987) 2059–2062.

[10] S. John, Strong localization of photons in certain disordered dielectric superlattices, *Physical Review Letters* 58 (1987) 2486–2489.
[11] K.M. Ho, C.T. Chan, C.M. Soukoulis, Existence of a photonic gap in periodic dielectric structures, *Physical Review Letters* 65 (1990) 3152–3155.
[12] M.S. Kushwaha, P. Halevi, L. Dobrzynski, B. Djafari-Rouhani, Acoustic band-structure of periodic elastic composites, *Physical Review Letters* 71 (13) (1993) 2022–2025.
[13] M. Sigalas, E.N. Economou, Band-structure of elastic-waves in 2-dimensional systems, *Solid State Communications* 86 (3) (1993) 141–143.
[14] M.S. Kushwaha, Classical band structure of periodic elastic composites, *International Journal of Modern Physics B* 10 (9) (1996) 977–1094.
[15] G.S. Gupta, Natural flexural waves and the normal modes of periodically-supported beams and plates, *Journal of Sound and Vibration* 13 (1970) 89–101.
[16] D.J. Mead, Wave propagation in continuous periodic structures: research contributions from Southampton, *Journal of Sound and Vibration* 190 (3) (1996) 495–524.
[17] R.S. Langley, The response of two dimensional periodic structures to point harmonic forcing, *Journal of Sound and Vibration* 197 (4) (1996) 447–469.
[18] R. Esquivel-Sirvent, G.H. Cocoletzi, Band-structure for the propagation of elastic-waves in superlattices, *Journal of the Acoustical Society of America* 95 (1) (1994) 86–90.
[19] M.R. Shen, W.W. Cao, Acoustic bandgap formation in a periodic structure with multilayer unit cells, *Journal of Physics D-Applied Physics* 33 (10) (2000) 1150–1154.
[20] P.G. Martinsson, A.B. Movchan, Vibrations of lattice structures and phononic band gaps, *Quarterly Journal of Mechanics and Applied Mathematics* 56 (1) (2003) 45–64.
[21] N.A. Day, C. Zhu, V.K. Kinra, A study of dispersive waves propagation in periodic layered composites, in: *Proceedings of Review of Progress in Quantitative Nondestructive Evaluation*, Brunswick, Maine, Plenum Press, New York, 1994, pp. 243–250.
[22] W.W. Cao, W.K. Qi, Plane-wave propagation in finite 2-2-composites, *Journal of Applied Physics* 78 (7) (1995) 4627–4632.
[23] A. Bedford, D.S. Drumheller, *Introduction to Elastic Wave Propagation*, Wiley, Chichester, 1994.
[24] J.S. Jensen, Phononic band gaps and vibrations in one- and two-dimensional mass-spring structures, *Journal of Sound and Vibration* 266 (5) (2003) 1053–1078.
[25] M.I. Hussein, G.M. Hulbert, R.A. Scott, Band-gap engineering of elastic wave guides using periodic materials, in: *Proceedings of the 2003 ASME International Mechanical Engineering Congress and R&D Expo*, Washington, DC, ASME Publication, New York, 2003, pp. 799–807.
[26] M.I. Hussein, Dynamics of Banded Materials and Structures: Analysis, Design and Computation in Multiple Scales, Ph.D. Thesis, University of Michigan, Ann Arbor, Michigan, 2004.
[27] M.I. Hussein, G.M. Hulbert, R.A. Scott, Effects of "finiteness" on wave propagation and vibration in elastic periodic structures, in: *Proceedings of the 2004 ASME International Mechanical Engineering Congress and R&D Expo*, Anaheim, California, ASME Publication, New York, 2004, pp. 437–447.
[28] J.P. Dowling, H. Everitt, E. Yablonovitch, Photonic and sonic band-gap bibliography [Online], http://www.pbglink.com.
[29] Mathworks Corp., MATLAB Technical Computing Environment [Online], http://www.mathworks.com.